Drug Development and Industrial Pharmacy, 27(10), 1017–1030 (2001)

RESEARCH PAPER

Characterization of the Solubility and Dissolution Properties of Several New Rifampicin Polymorphs, Solvates, and Hydrates

Stanley Q. Henwood,[1,*] Wilna Liebenberg,[1] Lourens R. Tiedt,[2] Antonie P. Lötter,[1] and Melgardt M. de Villiers[3,*]

[1]*Research Institute for Industrial Pharmacy and* [2]*Laboratory for Microscopy, Potchefstroom University for Christian Higher Education, Potchefstroom, 2520, South Africa*
[3]*Department of Basic Pharmaceutical Sciences, College of Pharmacy, University of Louisiana at Monroe, Monroe, Louisiana*

ABSTRACT

Based on reports that tuberculosis is on the increase, this investigation into the physicochemical properties of rifampicin when recrystallized from various solvent systems was undertaken. Rifampicin is an essential component of the currently recommended regimen for treating tuberculosis, although relatively little is known about its solubility and dissolution behavior in relation to its solid-state properties. A rifampicin monohydrate, a rifampicin dihydrate, two amorphous forms, a 1:1 rifampicin:acetone solvate, and a 1:2 rifampicin:2-pyrrolidone solvate were isolated and characterized using spectral, thermal, and solubility measurements. The crystal forms were relatively unstable because except for the 2-pyrrolidone solvate, all the hydrated or solvated materials changed to amorphous forms after desolvation. Fourier transform infrared (FTIR) analysis confirmed the favorable three-dimensional organization of the pharmacophore to ensure antibacterial activity in all the crystal forms except the 2-pyrrolidone

*Corresponding authors. Melgardt M. De Villiers, Ph.D., Associate Professor of Pharmaceutics, College of Pharmacy, University of Louisiana at Monroe, 700 University Avenue, Monroe, LA 71209. Fax: (318) 342 3255; E-mail: pydevilliers@ulm.edu

solvate. In the 2-pyrrolidone solvate, the strong IR signals of 2-pyrrolidone interfered with the vibrations of the ansa group. The 2-pyrrolidone solvate was the most soluble in phosphate buffer at pH 7.4. This solvate also had the highest solubility (1.58 mg/ml) and the fastest dissolution in water. In 0.1 M HCl, the dihydrate dissolved the quickest. A X-ray amorphous form (amorph II) was the least soluble and had the slowest dissolution rate because the powder was poorly wettable and very electrostatic.

Key Words: *Dissolution; Hydrates; Polymorphs; Rifampicin; Solubility; Solvate*

INTRODUCTION

Reports from the Centers for Disease Control and Prevention (CDC) in the United States state that, worldwide, tuberculosis takes about 2 million lives, and 8 million new cases are reported each year (1). Tuberculosis—the captain of all men of death, a scourge of 19th century Europe, a terrible memory of prewar generations—has resurfaced as a public health concern in the industrialized and developing world (2,3).

For tuberculosis treatment, at least four, or as many as seven, drugs are used, depending on the extent of the disease and the efficacy of available drugs (4,5). The four drugs of choice for initial treatment are isoniazid, rifampicin, pyrazinamide, and either streptomycin or ethambutol. However, bioavailability and clearance of most antibacterial drugs, but especially rifampicin, is unpredictable (6,7). Malabsorption of rifampicin (rifampin) is particularly common in those with acquired immunodeficiency syndrome (AIDS) and undernourished patients (8).

One possible cause for rifampicin bioavailability problems could be differences in the physicochemical properties of the drug (7,9,10). In our laboratory, we found that the differential scanning calorimetry (DSC) thermograms for several commercially available raw materials showed several endo-exothermic events in a broad range of temperatures, with a decomposition temperature of 249°C (11). This behavior is typical of a mixture of different crystal forms. According to Pelizza et al. (12), rifampicin shows polymorphism, which is believed to be due to the various possibilities for hydrogen bonding, conformational exchanges, and ionization states that allow different crystalline packings of the complex structure.

To date, the characterization of the standard product (form II), a solvate with 5 molecules of water of crystallization, another polymorph (form I), an amorphous phase, another solvate with 5 molecules of water, a one-ninth tetrahydrofuran solvate, and a 1:1 carbon tetrachloride solvate were reported for rifampicin (12–14).

In the literature, little information is given about the solubility and dissolution behavior of rifampicin in relation to its solid-state properties. This investigation into the crystal properties of rifampicin, when recrystallized from different organic solvents, reports solubility and dissolution differences for rifampicin polymorphs, solvates, hydrates, and amorphous forms. Methods to prepare and characterize these crystal forms are also given.

EXPERIMENTAL

Materials

Pure rifampicin was obtained from Yuhan Corporation, Seoul, Korea (batches 5108 and 5107, manufacturing date 05-07-1995; 99.6% by high-performance liquid chromatographic [HPLC] assay). This powder was characterized as form II (12). The water used was distilled and deionized through a Milli-Q system (Millipore, Milford, MA). All other materials and solvents were analytical grade (Table 1).

Preparation of Rifampicin Crystal Forms

Two general recrystallization methods were used to crystallize small or large amounts of crystals from different solvents. Small amounts of crystals, ± 1 g, were prepared by heating 80 ml of the solvent to 60°C. Rifampicin powder was added under

Table 1

Thermal Characteristics of Rifampicin Crystal Forms Obtained by Differential Scanning Calorimetry

Crystal Form	Solvent of Recrystallization	Stoichiometry	Dehydration/ Desolvation (°C)	Melting Endotherm (°C)	Exo/ Endotherm (°C)	Decomposition (°C)
Form II	—	—	—	—	193–203	251
Monohydrate	Ethanol	1:1	107	154	~192	223
Dihydrate	Benzene	1:2	97	183	—	221–249
Acetone solvate	Acetone	1:1	100	171	—	227
2-Pyrrolidone solvate	2-Pyrrolidone	1:2	79, 129	197	—	—
Amorph I	*n*-Butanol	—	—	114	165–205	219
Amorph II	Propionic acid:THF (10:90)	—	—	151	~200	192–220

THF, tetrahydrofuran.

constant stirring until a saturated solution was obtained. The solutions were left at room temperature to evaporate. Recrystallized and precipitated material was removed and dried under vacuum. Larger amounts of crystals, ±10 g, were prepared by evaporating 250 ml of saturated solutions in a Buchi Rotavapor R110 (Buchi, Flawil, Switzerland). The recrystallized material was removed from the flask and dried under vacuum for 24 h.

Thermal Analysis

Thermograms were measured with a differential scanning calorimeter (DSC) (Shimadzu DSC 50, Shimadzu, Kyoto, Japan). The instrument was calibrated with 5 mg of indium at a heating rate of 10°C/min (onset temperature 155.8°C, peak maximum 156.5°C, and heat of transitions 28.8 J/g). The thermal behavior (Table 1) was studied by heating ±5 mg of the powdered samples at a rate of 10°C/min from 30°C to 300°C in a hermetically sealed pan with a pinhole in the lid under a nitrogen purge of 20 ml/min. Thermogravimetric analysis (TGA) thermograms were recorded with a Shimadzu TG 50 system. Mass loss from ±10 mg samples at a heating rate of 10°C/min under nitrogen purge was recorded.

Fourier Transform Infrared Spectroscopy

The KBr disks were prepared by triturating 1–2 mg samples with 300–400 mg of dried, finely powdered potassium bromide and compressing 13-mm disks at a pressure of 10 kN. The disks were then mounted in a Shimadzu FTIR-4200 spectrophotometer and scanned from 4000 to 400 cm^{-1}. FTIR spectra were also obtained using a diffuse reflectance (DRFTIR) attachment. For DRFTIR analysis, the samples were mixed with finely powdered potassium bromide and screened through a 250-μm sieve. The measuring conditions were as follows: 2.0 resolution; 20 sample scan; single-sided acquisition.

X-Ray Powder Diffraction

X-ray powder diffraction (XRPD) diffractograms were recorded on an automated Philips PM 9901/00 diffractometer using CuK_α radiation ($\lambda = 1.54051$ Å) and a scan speed of 2° 2θ/min (Philips, Eindhoven, The Netherlands). The samples were finely ground and screened through a 250-μm sieve before being packed into standard aluminum sample holders. This eliminated the preferred orientation of crystals during analysis. The powder patterns were recorded under the following conditions: 40 kV, 30 mA; range 10^4 cps; time constant 4; angular range 5–40° 2θ; divergence slit 1°; scatter slit 0.2°; receiving slit 1°.

Scanning Electron Microscopy

Scanning electron microscopy (SEM) micrographs of the crystals and powder were obtained using a Philips XL 30 scanning electron microscope. Samples were mounted on a metal stub with an adhesive layer and then first coated under vacuum with carbon (Emscope TB500 sputter-coater, Cambridge, England) before being coated with a

thin gold-platinum film (Eiko Engineering Ion Coater IB-2, Tokyo, Japan).

Solubility Determination

To determine the solubility in water, 12-ml vials containing distilled, deionized water and excess amounts of each crystal form were rotated (350 rpm) in a water bath kept at 30°C ± 0.1°C. After 48 h, equilibrium was reached, and aliquots of the solution were withdrawn from the vials and filtered through a 0.25-μm filter. The solutions were suitably diluted with methanol and assayed spectrophotometrically at 333 nm. Results are the mean of three determinations.

Powder Dissolution Measurements

Powder dissolution rates were determined according to the method described by Lötter et al. (15). In this method, powder aggregates are first dispersed by sonification with 0.1-mm glass beads. The dissolution media used were 900 ml water, 0.1 M HCl or phosphate buffer at pH 7.4; these were kept at 37°C and stirred at 100 rpm. The rifampicin content in the dissolution medium was spectrophotometrically determined at 333 nm after suitable dilution with methanol. The crystals and powders were prescreened to isolate particles between 0 and 250 μm for dissolution testing. Similarity factors were calculated to compare the dissolution profiles (16).

Moore and Flanner (16) introduced the similarity factor as a simple model-independent approach using mathematical indices to define differences and similarities between dissolution profiles. These factors are divided from Minkowski differences (average absolute differences) and mean-square difference, respectively. In this study, a similarity factor was calculated using the following mathematical equation (17,18):

$$f_2 = 50 \bullet \log\left(\left[1 + \left(\frac{1}{n}\right)\sum_{t=1}^{n} w_t(R_t - T_t)^2\right]^{-0.5} \bullet 100\right) \quad (1)$$

where n is the number of dissolution time points; R_t and T_t are the reference and test dissolution values at time t, respectively; and w_t is an optional weighting factor. The value of f_2 is 100 when the test and reference mean profiles are identical. The test and reference products are not equivalent when there is more than 10% difference in dissolution profiles, indicated by a similarity factor smaller than 50 (16).

RESULTS AND DISCUSSION

Gadret et al. (13), Gallo et al. (14), and Pelizza et al. (12) reported studies concerning the crystal properties of rifampicin. These studies described the preparation and characterization of a number of rifampicin crystal forms, which were also successfully prepared in this study. However, after several crystallization trials, a rifampicin monohydrate, dihydrate, acetone solvate, 2-pyrrolidone solvate, and two amorphous forms were repeatedly isolated. The morphological, thermal analysis, XRPD, infrared spectroscopic, solubility, and dissolution properties of these crystal forms were measured.

Crystal Morphology

On close visual inspection of the crystal forms, definite differences in morphology were evident among the powders. The differences were confirmed by studying the shape and appearance of crystal forms with a scanning electron microscope (Fig. 1).

The rifampicin monohydrate obtained from absolute ethanol was small, platelike crystals. From benzene, ethyl acetate, and tetrahydrofuran, platelike particles with smaller undefined particles inbetween were crystallized. This was a rifampicin dihydrate. The crystal structure of the acetone solvate crystals was not clearly defined, and their surfaces were uneven. The appearance of both small and large particle size fractions was clear from the photomicrograph of this powder. The crystals of the 2-pyrrolidone solvate were irregularly shaped, platelike crystals that were closely packed. Amorphous particles, crystallized from *n*-butanol and 10% propionic acid in tetrahydrofuran solution, showed no definite crystal structure, and the particles were undefined and glasslike with smooth sides.

X-Ray Powder Diffraction Results

It is well known that XRPD is a powerful technique for the identification of crystalline and noncrystalline phases. This technique therefore was employed to establish differences in crystal form.

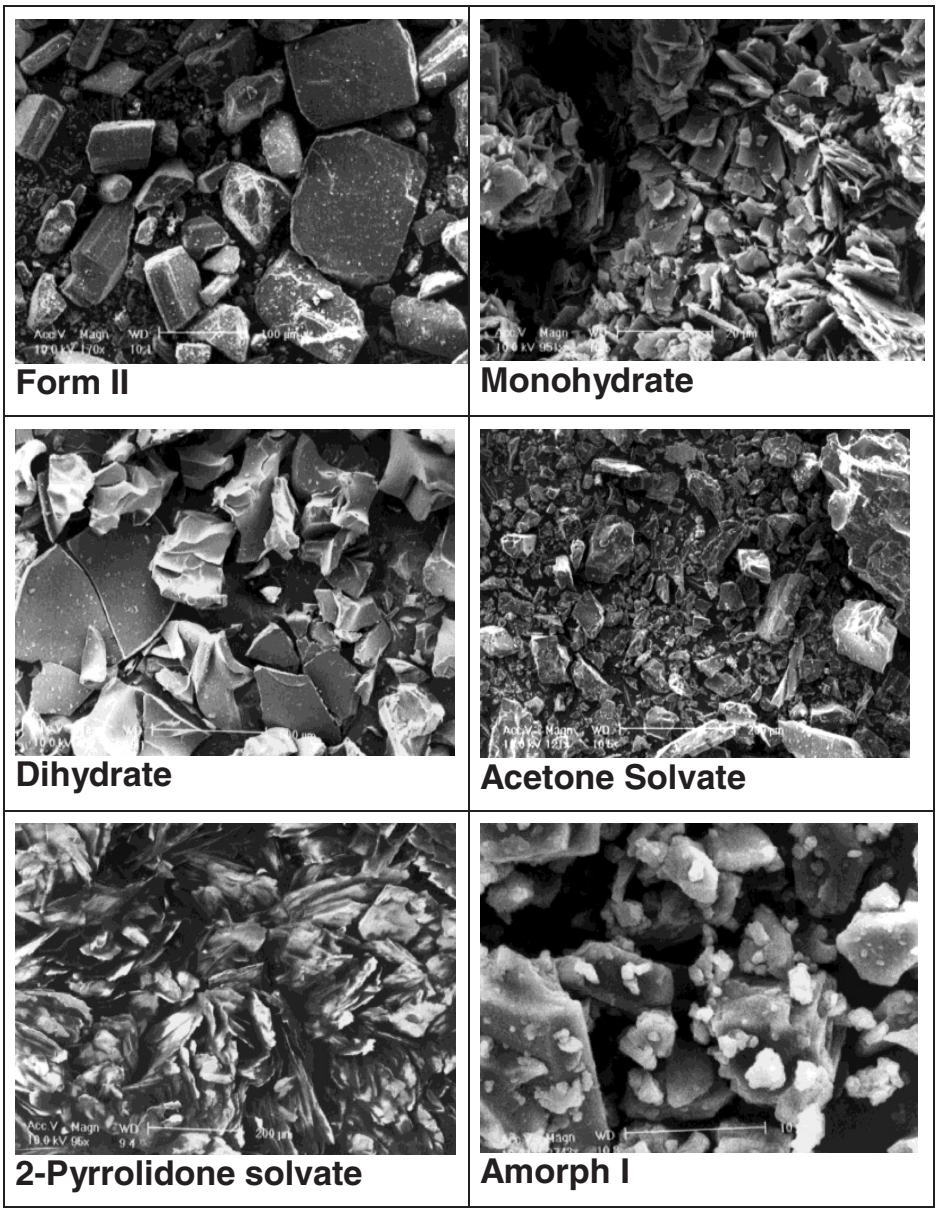

Figure 1. SEM photomicrographs of rifampicin crystal forms.

Gallo and Radaelli (14) reported the XRPD pattern of form II, and the raw material used for recrystallization in this study had the same pattern (Fig. 2). Grinding caused the crystallinity of rifampicin form II to disappear and an amorphous form to originate.

In Fig. 2, the diffractograms of the recrystallized materials are given. After drying at 70°C for 2 h, all the diffractograms except that of the 2-pyrrolidone solvate were the characteristic halo shape of amorphous material similar to amorph I (Fig. 2). The characteristic d values and relative intensities (I/I_{max}) of the major peaks were compared with those previously reported for the anhydrate (form II) (12,14).

Each crystal form had a distinct and characteristic XRPD pattern, which only changed after transformation of the crystals, such as desolvation or

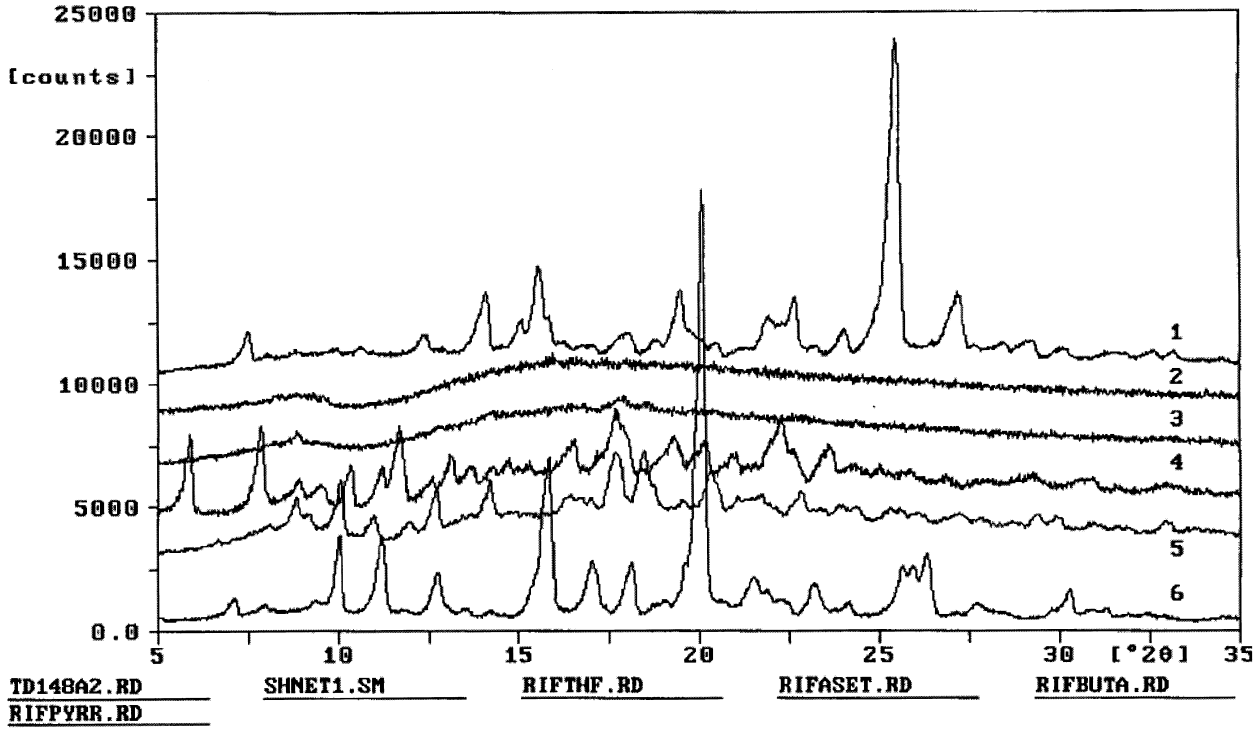

Figure 2. XRPD patterns of rifampicin powders recrystallized from various solvent systems: (1) 2-pyrrolidone solvate; (2) amorph I; (3) acetone solvate; (4) dihydrate; (5) monohydrate; (6) form II.

dehydration. For example, on drying at 70°C for 2 h, the crystalline powder of the dihydrate with a relatively high degree of crystallinity was changed to a less crystalline phase because there was a sharp drop in peak intensity; the counts per second dropped from 3434 to 331 at $(I/I_{max}) = 100\%$. The less-crystalline phase was not structurally identical to that of the hydrated phase.

Because of its physical instability, it was not easy to record the XRPD pattern of the monohydrate. The diffractogram, however, did show some characteristics of a crystalline powder, but the high background values in relation to peak intensities (counts/second) indicated the presence of a predominantly amorphous phase. After drying, the powder was completely amorphous with no discernible peaks. This was also true for the XRPD pattern of the acetone solvate.

Compared to the monohydrate, the acetone solvate was relatively stable because the relative intensity values after drying, although at relatively lower counts, were similar to that of the solvated powder. This difference in peak intensity at $(I/I_{max}) = 100\%$ was only 400 counts/s. The XRPD pattern of the 2-pyrrolidone solvate is characteristic of a crystalline powder with a high degree of crystallinity. Removal of the solvent of crystallization changed the diffractogram, but it was still characteristic of a crystalline powder with a relatively high degree of crystallinity. The three main diffraction peaks moved to 3.45, 3.47, and 6.91 Å compared to 3.49, 5.67, and 4.55 Å for the solvate.

The XRPD patterns of the two amorphous forms had no discernible peaks, and only background values were recorded, which indicated the absence of crystalline phases. A lack of crystallinity was most probably caused by rapid precipitation during fast recrystallization in a water-free environment.

Thermal Properties

The DSC thermogram of form II (Fig. 3), which is predominantly the commercially available form,

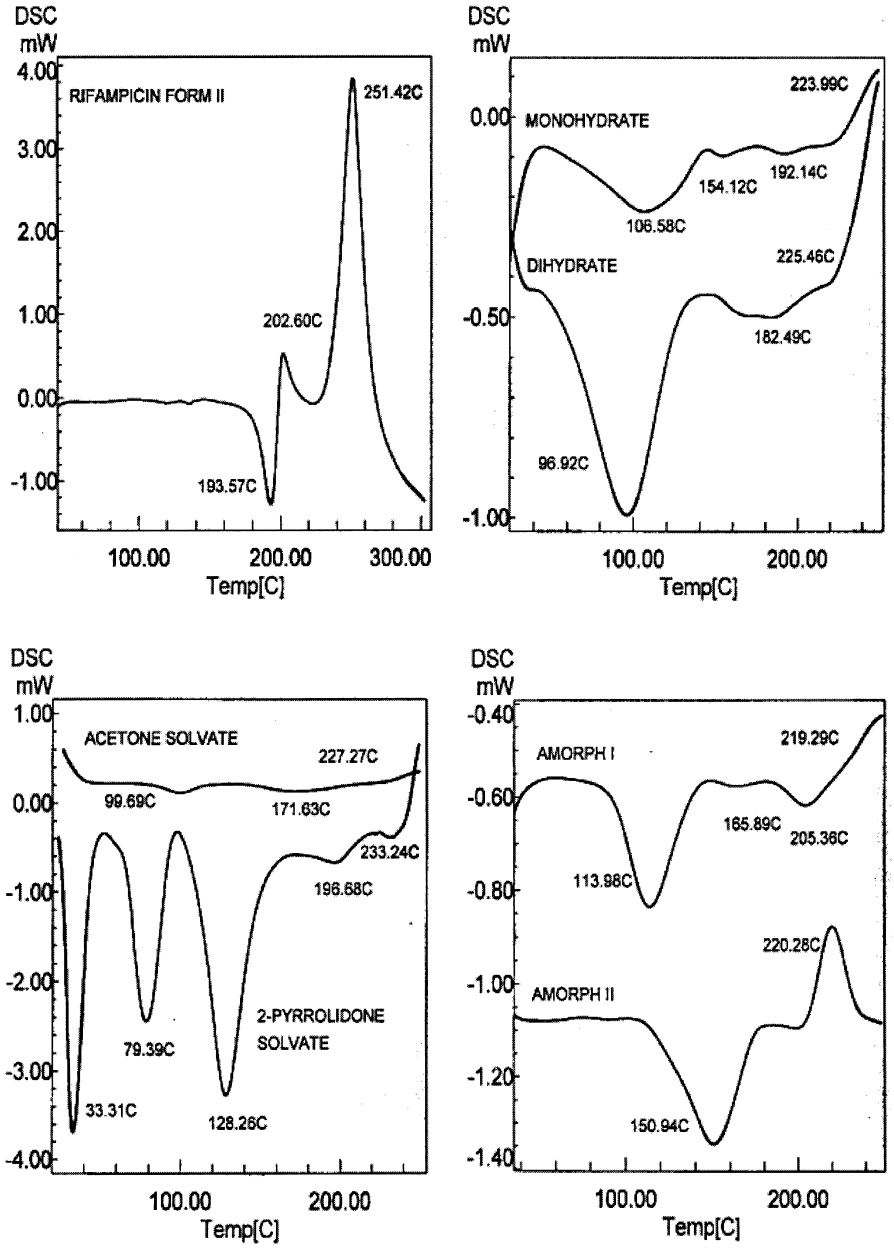

Figure 3. DSC thermograms of rifampicin powders recrystallized from various solvent systems.

showed an exo-endothermic process at 193°C–200°C, leading to a product that decomposes at 240°C.

The monohydrate recrystallized from ethanol (Fig. 3) showed a dehydration endotherm at 107°C, followed by a melting endotherm at 154°C (Table 1). This was followed by an endo-exothermic process at around 192°C, which was interpreted as melting and recrystallization of the dehydrated form into a glasslike product that decomposed at 223°C. These crystals were a monohydrate because the TGA weight loss (Fig. 4 and Table 2) was 2.1%. This is not stoichiometrically equivalent to the loss of solvent, but rather to the loss of one molecule of water.

DSC thermograms obtained for the dihydrates recrystallized from a number of solvents showed a desolvation endotherm in the temperature range

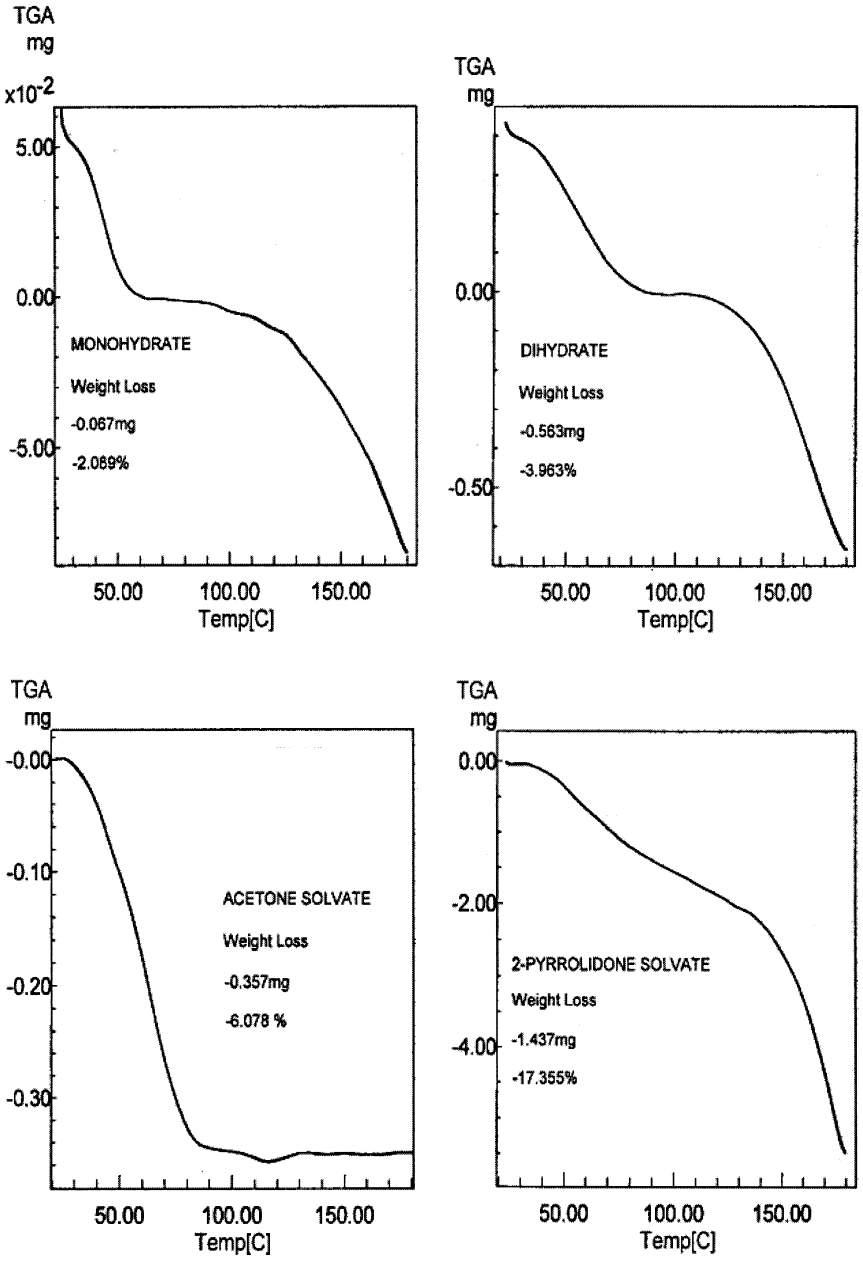

Figure 4. TGA results for a number of rifampicin hydrates and solvates.

from 41°C to 138°C (Table 3). This was followed by a melting endotherm at 183°C. Decomposition ranged from 221°C to 249°C. As indicated in Table 3 and Fig. 4, weight loss from rifampicin dihydrates ranged from 3.7% to 4.0%. The formation of solvates was eliminated because theoretical weight loss based on the stoichiometry of solvent:rifampicin ratios did not correspond to experimental values. The mean measured weight loss correlated best with the calculated weight loss of 4.2% for a dihydrate. The difference could be the result of the relative instability of the dihydrate because dehydration started to occur at very low temperatures (Figs. 3 and 4).

The acetone solvate showed a desolvation endotherm at 40°C–117°C, corresponding to the

Table 2

Thermogravimetric Analysis Weight Loss Data for Rifampicin Monohydrate, Acetone Solvate, and 2-Pyrrolidone Solvate

Solvent of Crystallization	Theoretical Stoichiometry	Weight Loss (%)	Range (°C)	Theoretical Weight Loss (%)	Measured Stoichiometry
Monohydrate	1:1	2.1	35–125	2.1	1:1.00
Acetone	1:1	6.1	40–117	6.6	1:0.92
2-Pyrrolidone	1:2	17.4	65–139	17.1	1:1.02

Table 3

Thermogravimetric Analysis Weight Loss from Rifampicin Dihydrates with Similar X-Ray Powder Diffraction Patterns Crystallized from Different Solvents

Solvent of Recrystallization	Weight Loss (%)	Range (°C)	Theoretical Weight Loss (%)	Measured Stoichiometry
Tetrahydrofuran	3.7	42–138	4.2	1:0.88
Benzene	4.0	45–125	4.2	1:0.95
Ethyl acetate	4.0	41–131	4.2	1:0.95
Dimethylformamide	3.9	45–127	4.2	1:0.93

loss of one acetone molecule from a 1:1 rifampicin:acetone solvate. Desolvation was followed by a melting endotherm at 171°C. No endo-exothermic process was detected before decomposition at 227°C (Fig. 3). A melting endotherm at 33°C attributed to residual 2-pyrrolidone, two desolvation endotherms (at 79°C and 129°C), and a melting endotherm at 197°C; no decomposition endotherm was observed for the 2-pyrrolidone solvate. The disappearance of the decomposition endotherm suggested that desolvation changed the crystal form to a very stable crystalline phase, as seen by XRPD analysis. TGA analysis showed that the 2-pyrrolidone solvate had a stoichiometry of 1:2, and a combination of DSC (Fig. 3) and TGA (Fig. 4) data confirmed that desolvation occurred in two distinct processes.

In the thermograms of an amorphous form crystallized from *n*-butanol (amorph I), a melting endotherm at 114°C and decomposition at 219°C–243°C were seen (Fig. 3). This form contained no water of imbibition or crystallization. The second amorph (II) displayed a melting endotherm at 151°C, with a large exotherm at 188°C–220°C (Fig. 3). This decomposition exotherm starting at 188°C is lower than that for amorph I and could possibly be explained by the fact that the degree of crystallinity (Fig. 2) was different for the two amorphous powders.

Fourier Transform Infrared Spectroscopy

The interpretation of the IR spectra of the various forms of rifampicin was based on the spectra of a series of rifampicin monologues (19), rifampicin in solution (14), and reported rifampicin crystal forms (12). FTIR assignments were made based on comparison of the spectra of the various crystal forms compressed in KBr disks or using DRFTIR spectroscopy. From these results, three distinct regions in the IR spectrum of rifampicin were identified as characteristic IR vibrations due to the amide moiety, chromophore, and the ansa chain (Fig. 5). The assignments of the characteristic frequencies of the amide moiety in the different crystal forms are listed in Table 4. The assignment of characteristic vibration of the pharmacophore (ansa C_{20} to C_{27}; Fig. 5) is listed in Table 4. The relationship between antibiotic activity and chemical properties of rifampicin has been extensively studied, and a phenomenological model indicating the requirement for activity has been suggested (20). In particular, the mechanism of action of rifampicin against bacterial DNA-dependent RNA polymerase has been explained on the basis of the spatial arrangement of the four oxygen molecules of the ansa chain that forms hydrogen bonds with the enzyme. All this is mostly regulated by the position of the C_{34} (Fig. 5).

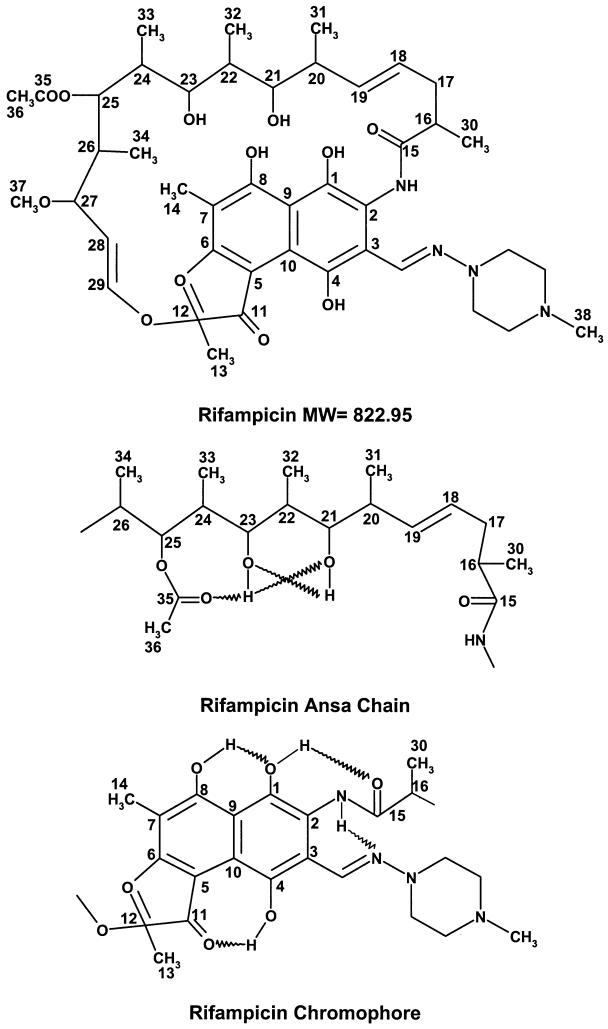

Figure 5. Molecular structures of rifampicin, with the chromophore and ansa chain showing the various hydrogen-bonding possibilities.

For rifampicin, an important part of the ansa chain is the acetyl group at C_{25}, which exhibits bands in three regions of the spectrum corresponding to ν C=O, ν asym C–O–C, and ν sym C–O–C. Based on deuteration studies, the ν C=O is the vibration accepted for the hydrogen bond of the C_{23}–OH. The presence and absence of chelation are indicated by a low ($\sim$1705 cm^{-1}) or high ($\sim$1740 cm^{-1}) frequency, respectively.

For the crystal forms studied, the presence or absence of the vibration due to the ν C=O group explained the hydrogen bonding of the C_{23}–OH to the acetyl group on C_{25} (Table 4). This vibration was present in all the studied crystal forms except the 2-pyrrolidone solvate. The dihydrate and acetone solvate showed both the low-frequency and the high-frequency peaks in DRFTIR spectra, suggesting that there might be crystals with and without chelation. Since these forms were less crystalline, as seen from XRPD and thermal analysis data, this might explain the presence of both bands. In all the crystal forms except possibly the 2-pyrrolidone solvate, IR vibrations confirmed the favorable local arrangement of the C_{20} to C_{27} section of the ansa chain via a system of intramolecular hydrogen bonds.

This interpretation of the ν C=O was supported by investigation of the ν OH bands in the region 3600–3400 cm^{-1}. By comparing the ν OH of rifampicin at 3560 cm^{-1} and 3460 cm^{-1} in the solid state with the 3450-cm^{-1} value in solution, it was concluded that predominantly the intramolecular hydrogen bond between C_{23}–OH and the acetyl group did not exist in the crystal forms. This conclusion agreed with the interatomic distances of the atoms concerned, obtained from X-ray data in the solid state for rifampicin form II and the pentahydrate (13,20).

Therefore, only the OH groups at C_{23} and C_{21} were intramolecularly hydrogen bonded. Although not observed for the crystal forms studied, it is possible that, in cases when the C_{23}–OH were hydrogen bonded to the acetyl group, it acted as a dual acceptor in the hydrogen bonding of the C_{21}–OH and the C=O. Other bands due to the ansa OH groups in the regions near 1300 cm^{-1} and 1100–900 cm^{-1} were assigned to a mixed vibration of δ OH–ν C–O (19).

Characteristic IR vibrations of other groups characteristic for rifampicin and the solvates were also identified. The IR band due to the piperazine N–CH_3 group of rifampicin is present in $CDCl_3$ solution at 2800 cm^{-1}, but was absent in all the crystal forms. This suggested that rifampicin exists as a zwitterion in all the crystal forms (19). Strong overtones in the region 3600–3400 cm^{-1}, leading to overlapped bands, might be the result of crystal water present in the monohydrate and dihydrate. The presence of acetone in acetone solvate crystals was confirmed by the very strong signal, with a mean absorbance of 0.97 $\pm$ 0.10 due to the ν C=O listed in Table 4. The IR spectrum of 2-pyrrolidone is dominated by the strong C=O peak at around 1700 cm^{-1}. This same peak dominated

Table 4

Characteristic Infrared Vibrations of the Amide, Chromophore, and Pharmacophore Observed in Rifampicin Crystal Forms

		Amide			Chromophore			Pharmacophore		
Crystal Form	IR-Method	ν N–H	Amide I	Amide II	ν C_{11}=O	ν C_1=O	ν OH	ν C=O	ν asym C–O–C	ν sym C–O–C
Form II[a]	KBr	3365	1670	—	1735	—	3300	1715	1255	1020
	DRFTIR	3345	1670	—	1735	—	3300	1715	1255	1020
Monohydrate	KBr	—	—	—	—	—	3300	1727	1241	1060
	DRFTIR	—	—	—	—	—	3300	—	—	—
Dihydrate	KBr	—	—	1534	1650	—	Overlap	1725	1247	1023
	DRFTIR	—	—	1534	1738	—	3300	1725	1248	1023
Acetone solvate	KBr	—	—	1536	1652	—	Overlap	1711	—	1023
	DRFTIR	3353	—	1538	1738	—	3300	1708	1252	1027
2-Pyrrolidone solvate	KBr	3347	1680	—	—	—	3300	—	1260	—
	DRFTIR	—	1694	1515	1694	—	3300	—	1262	—
Amorph I	KBr	—	1708	1536	1650	—	3300	1710	1245	1025
	DRFTIR	—	1708	1540	1738	—	3300	1725	1248	1025
Amorph II	KBr	—	1708	1534	1652	—	3300	1725	1245	1025
	DRFTIR	—	1706	1538	1733	—	3300	1725	1245	1027

—Not observed. DFTIR, diffuse reflectance attachment Fourier transform infrared.
[a]According to Ref: 19.

the IR spectrum of the 1:2 2-pyrrolidone solvate (Table 4).

Solubility of Rifampicin Crystal Forms in Water

Solubilities of the different crystal forms in water were determined and then compared statistically using the Student-Newman-Keuls multiple range tests. Solubility data in water at 30°C ± 1°C are listed in Table 5. The solubilities of the different crystal forms ranged from 0.20 ± 0.077 mg/ml for amorph II to 1.58 ± 0.006 mg/ml for the 2-pyrrolidone solvate. Standard deviations ranged from 0.14% to 9.50%. Based on statistical analysis, the solubility of amorph II was significantly lower than that of the other crystal forms. Form II and the 2-pyrrolidone solvate were the most soluble crystal forms.

Effect of Dissolution Medium on the Dissolution Rate of Rifampicin Crystal Forms

Similarity factors for the dissolution of the crystal forms in different dissolution media are listed in Table 6. The similarity factor f_2 and a similarity testing criteria based on f_2 are recommended for dissolution profile comparison in the FDA's guidelines for industry (17,18). Dissolution profiles of the different crystal forms in each of the dissolution media are shown in Figs. 6 to 8. The dissolution profiles of the 2-pyrrolidone solvate, amorph I, the dihydrate, and the monohydrate were not different

Table 5

Solubility of Rifampicin Crystal Forms in Water at 30°C

Crystal Form	Solubility (mg/ml)	Standard Deviation (mg/ml)	P[a]
Form II	1.472	0.006	.00171
Monohydrate	0.874	0.058	.00015
Dihydrate	0.982	0.004	.00019
Acetone solvate	0.732	0.001	.00016
2-Pyrrolidone solvate	1.576	0.006	—
Amorph I	0.897	0.005	.00019
Amorph II	0.195	0.077	.00018

[a]Solubilities compared to the highest solubility (2-pyrrolidone solvate) at a 95% confidence interval (Student-Newman-Keuls multiple range test).

Table 6

Similarity Factors f_2 for Dissolution Profiles of Different Crystal Forms in Different Dissolution Media

Crystal Form	Compared with 2-Pyrrolidone Solvate Buffer pH 7.4[a]	Compared with Dihydrate 0.1 M HCl	Compared with 2-Pyrrolidone Solvate Water
Form II	31.94	48.88	32.19
Monohydrate	36.14	71.92	38.52
Dihydrate	18.21	100.00	15.72
Acetone solvate	17.77	54.19	10.99
2-Pyrrolidone solvate	100.00	43.45	100.00
Amorph I	19.13	47.45	15.69
Amorph II	6.13	11.07	9.28

[a]Test and reference are not equivalent when there is a 10% difference in dissolution profiles ($f_2 < 50$).

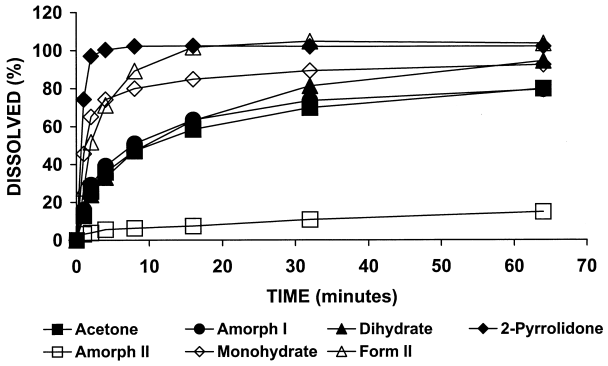

Figure 6. Dissolution profiles in phosphate buffer pH 7.4 of rifampicin powders recrystallized from various solvents.

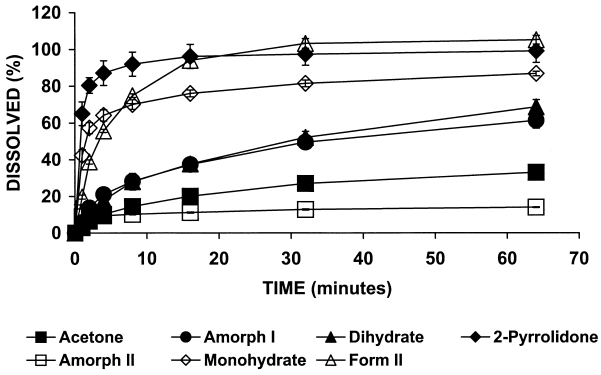

Figure 8. Dissolution profiles in water of rifampicin powders recrystallized from various solvents.

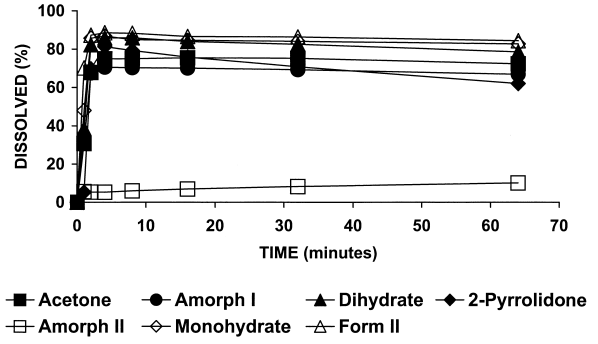

Figure 7. Dissolution profiles in 0.1 M HCl of rifampicin powders recrystallized from various solvents.

in buffer at pH 7.4, 0.1 M HCl, or water. However, dissolution was the fastest in 0.1 M HCl, followed by buffer at pH 7.4, and then water. For example, the dissolution rate of the monohydrate in 0.1 M HCl was equal to the dissolution rate in the buffer ($f_2 = 53.27$), which was equal to the dissolution rate in water ($f_2 = 58.88$). However, the dissolution rate in water was different from the rate in 0.1 M HCl ($f_2 = 44.36$). Amorph II was the least soluble in all three media (less than 20% powder dissolved after 64 min), but it had the highest dissolution rate in water, followed by the buffer and 0.1 M HCl. The dissolution rates of the 2-pyrrolidone solvate were the fastest in both the buffer and water. In 0.1 M HCl, the dihydrate dissolved the quickest, significantly faster than the 2-pyrrolidone solvate ($f_2 = 15.72$).

In buffer at pH 7.4, the dissolution rates of the crystal forms (Fig. 6), from the fastest to the slowest according to the similarity factors, were as follows: 2-Pyrrolidone solvate > Monohydrate > Form II > Amorph I ≥ Dihydrate ≥ Acetone solvate > Amorph II.

The dissolution rates of the crystal forms in 0.1 M HCl (Fig. 7), from the fastest to the slowest, were as follows: Dihydrate ≥ Monohydrate > Acetone solvate > Form II > Amorph I ≥ 2-Pyrrolidone solvate > Amorph II.

Finally, the dissolution rates of the crystal forms in water (Fig. 8), from the fastest to the slowest, were as follows: 2-Pyrrolidone solvate > Monohydrate > Form II > Amorph I ≥ Dihydrate > Acetone solvate > Amorph II.

CONCLUSIONS

In light of the resurgence of tuberculosis and because rifampicin is still preferred for treating this disease in many patients, it is hoped that the results of this study will increase the understanding that problems associated with the solid-state properties of this drug might determine the in vivo performance of dosage forms.

The crystal form of rifampicin changed quite easily when crystallized from a wide range of solvent systems. A rifampicin monohydrate, dihydrate, two amorphous forms, an acetone solvate, and 2-pyrrolidone solvate were isolated and characterized using spectral, thermal, and solubility measurements. The crystal forms, however, were relatively unstable because, except for the 2-pyrrolidone solvate, all the hydrated or solvated materials changed to amorphous forms after desolvation.

FTIR analysis confirmed the three-dimensional organization of the pharmacophore to ensure activity against bacterial DNA-dependent RNA polymerase in all the crystal forms except the 2-pyrrolidone solvate. Especially, the favorable local arrangement of the C_{20}–C_{27} section of the ansa chain was granted by a system of intramolecular hydrogen bonds. It may be possible that 2-pyrrolidone solvate is inactive because this arrangement was not observed, but more likely, the strong IR signals of 2-pyrrolidone interfered with the vibrations of the ansa group.

FTIR results also showed that intramolecular hydrogen bonding between the NH group and the piperazine side chain existed in most crystal forms. Possible chelation of the C_1=O with the C_8 hydroxyl group was indicated by the absence of the C_1=O vibration in all the crystal forms. All this suggested that rifampicin existed as a zwitterion in the crystal forms.

The solubility and dissolution rates of the different crystal forms in aqueous solutions were significantly different. The 2-pyrrolidone solvate was the most soluble in phosphate buffer at pH 7.4, while amorph II was the least soluble. Since this solvate also had the highest solubility and the fastest dissolution in water, it was considered as being the crystal form with the best overall dissolution behavior. However, taking into consideration that dissolution in 0.1 M HCl simulates the behavior of rifampicin in the stomach, it could be argued that the dihydrate would have the best in vivo performance.

Although it is accepted in theory that amorphous forms should have a faster dissolution rate and a higher solubility than crystalline forms, amorph II was very poorly soluble and had the slowest dissolution rate in all dissolution media tested. This might be explained by the fact that the powder of amorph II was poorly wettable and very electrostatic. This problem could be eliminated by the addition of surfactants to solid dosage forms and dissolution media.

ACKNOWLEDGMENT

We would like to thank the National Research Foundation of South Africa (NRF) for financial support and Rolab Pharmaceuticals for generous donations of rifampicin.

REFERENCES

1. Castro, K.G. Newsletter: Tuberculosis Elimination. TB Notes **1999**, *3*, 1–2.
2. World Health Organization. *World Health Organisation, Global Tuberculosis Programme, Report Global Tuberculosis Control*; World Health Organization: Geneva, Switzerland, 1998; WHO/TB/98-237.
3. Sterling, T.R.; Alwood, K.; Gachuhi, R.; Goggin, W.; Blazes, D.; Bishai, W.R.; Chaisson, R.E. Relapse Rates After Short-Course (6-Month) Treatment of Tuberculosis in HIV-Infected and Uninfected Persons. AIDS **1999**, *13*(14), 1899–1904.
4. Mandell, G.L.; Petri, W.A. Antimicrobial Agents: Drugs Used in the Chemotherapy of Tuberculosis, *Mycobacterium avium* Complex Disease, and Leprosy. In *Goodman and Gilman's the Pharmacological Basis of Therapeutics*, 9th Ed.; Hardman, J.G., Limbird, L.E., Eds.; McGraw-Hill: New York, 1996; 1155–1174.

5. National Department of Health, South Africa. *Standard Treatment Guidelines and Essential Drug List for South Africa*. National Department of Health, South Africa: Pretoria, South Africa, 1996; 331 pp.
6. Männistö, P. Absorption of Rifampin from Various Preparations and Pharmaceutic Forms. Clin. Pharmacol. Ther. **1997**, *21*, 370–374.
7. Jindal, K.C.; Chaudhary, R.S.; Singal, A.K.; Gangwal, S.S.; Khanna, S. Effect of Particle Size on the Bioavailability and Dissolution Rate of Rifampicin. Indian Drugs **1994**, *32*, 100–107.
8. Douglas, J.G.; McLeod, M.J. Pharmacokinetic Factors in the Modern Drug Treatment of Tuberculosis. Clin. Pharmacokinet. **1999**, *37*, 127–146.
9. Ghabo, S.A.; Gognion, M.M.; Williamson, M.J. Modified Dissolution Method for Rifampin. Drug Dev. Ind. Pharm. **1989**, *15*, 331–335.
10. Ammar, H.O.; Khalil, R.M. Discrepancy Among Dissolution Rates of Commercial Tablets as a Function of Dissolution Method. Die Pharm. **1996**, *51*, 165–168.
11. Henwood, S.Q.; De Villiers, M.M.; Liebenberg, W.; Lötter, A.P. Solubility and Dissolution Properties of Generic Rifampicin Raw Materials. Drug Dev. Ind. Pharm. **2000**, *26*, 403–408.
12. Pelizza, G.; Nebuloni, M.; Ferrari, P.; Gallo, G.G. Polymorphism of Rifampicin. Il Farmaco **1977**, 32, 471–481.
13. Gadret, P.M.; Goursolle, M.; Leger, J.M.; Colleter, C. Structure Cristalline De La Rifampicine $C_{43}N_4O_{12}H_{58} \cdot 5H_2O$. Acta Cryst. **1975**, *B31*, 1454–1462.
14. Gallo, G.G.; Radaelli, P. Rifampin. In *Analytical Profiles of Drug Substances*; Florey, K., Ed.; Academic Press: New York, 1976; Vol. 5, 467–513.
15. Lötter, A.P.; Flanagan, D.R.; Palepu, N.R.; Guillory, J.K. A Simple Reproducible Method for Determining Dissolution Rates of Hydrophobic Powders. Pharm. Technol. **1983**, *7*, 55–66.
16. Moore, J.W.; Flanner, H.H. Mathematical Comparison of Dissolution Profiles. Pharm. Technol. **1996**, *20*, 64–74.
17. SUPAC-IR. *Guidance for Industry: Chemistry, Manufacturing, and Controls, In-Vitro Dissolution Testing, and In Vivo Bioequivalence Documentation*; Rockville, MD, 1995; 40 pp.
18. Food and Drug Administration. *Guidance for Industry, Dissolution Testing of Immediate Release Solid Oral Dosage Forms*; Food and Drug Administration: Rockville, MD, 1997; 30 pp.
19. Ferrari, P.; Gallo, G.G. Infrared Spectra of Rifamycins. Il Farmaco **1975**, *30*, 676–696.
20. Brufani, M.; Cerrini, S.; Fedeli, W.; Vaciago, A. Rifamycins: An Insight into Biological Activity Based on Structural Investigations. J. Mol. Biol. **1974**, *87*, 409–435.